Synthesis of dot in rod semiconductor heterostructures for the engineering of nanocrystals optical properties

Cite as: AIP Conference Proceedings **2416**, 020008 (2021); https://doi.org/10.1063/5.0069051
Published Online: 05 November 2021

Rocco Carcione, Francesca Limosani and Francesco Antolini

Synthesis of Dot in Rod Semiconductor Heterostructures for the Engineering of Nanocrystals Optical Properties

Rocco Carcione [a)], Francesca Limosani [b)], Francesco Antolini [c)]

ENEA C.R. Frascati Fusion and Nuclear Security Department, Division of Physical Technologies for Safety and Health, Photonics Micro and Nanostructures Laboratory, via E. Fermi 45, 00044 Frascati, Rome, Italy.

[c)] Corresponding author: francesco.antolini@enea.it
[a)] carcionerocco@gmail.com
[b)] limosani.lavoro@gmail.com

Abstract. This paper focuses on a preliminary study based on a two-steps approach to produce complex core/multiple shell architectures, such as "dots-in-rods" (DRs), to be exploited as color down-conversion filters for display manufacturing. Core/shell CdSe/CdS DRs are prepared by using a conventional fast hot injection reaction method to grow CdS layers onto CdSe QDs cores. Then, the CdSe/CdS DRs are engineered by growing an additional CdS shell coated by oleate (OA) molecules, thus producing CdSe/CdS@CdS/OA DRs. This further hybrid shell is synthesized by means of a seeded-growth approach, consisting of the controlled injection of TOP-S and cadmium oleate ($Cd(OA)_2$) as sulfur and cadmium precursors, respectively. As assessed by transmission electron microscopy (TEM) and UV-Vis absorption and photoluminescence (PL) spectroscopies analyses, the feasibility to control the amount of precursors allows to modulate the thickness of the further hybrid shells and therefore the morphological and optical properties of the final heterostructures. The introduction of further shells grafted by specific organic ligand improves the solubility in polymeric matrices. This condition is crucial to produce hybrid nanocomposite films that can be integrated in display manufacturing applications. Moreover, the capability of the final CdSe/CdS@CdS/OA nanostructures to convert blue light in red wavelengths with a remarkable photoluminescence quantum yields (PLQY) makes the produced materials the ideal candidates for a variety of optoelectronic applications, particularly for the fabrication of color down-conversion filters.

INTRODUCTION

In the last decades, the growing demand in display market focused the attention on the research of new strategies and materials to produce innovative and efficient devices. In particular, promising technologies for display manufacturing are interested in the fabrication of down-conversion systems, that showed great potential to realize color-stable red-green-blue (RGB) emission via blue LEDs or OLEDs [1,2]. The down-conversion process consists of the use of blue LEDs or OLEDs as pumping sources, that lead to emission of green or red light after the excitation of down-conversion materials by blue light.

In this context, semiconductor quantum dots (QDs) received particular attention as potential candidates for down-conversion processes [3] due to their high photoluminescence quantum yields (PLQY), color saturation related to narrow PL linewidth, and precisely tunable emission wavelengths based on the control of composition and size [4]. Moreover, the broad absorption spectra and beneficially high absorption capability in the near-UV–blue region provide high conversion efficiency [5]. Within the various semiconductor QDs, CdSe is the most studied colloidal nanocrystal system, owing to its high quality synthesis and its band gap of 1.84 eV, that allows to modulate the emission window of CdSe QDs in almost the whole visible spectral range via the control of their size [6–9].

NanoInnovation 2020
AIP Conf. Proc. 2416, 020008-1–020008-10; https://doi.org/10.1063/5.0069051
Published by AIP Publishing. 978-0-7354-4133-0/$30.00

However, the applications of CdSe QDs in optoelectronic devices are limited by the effects produced by their spherical shape on photophysical properties, such as blinking, spectral diffusion, long luminescence lifetime and unpolarized emission [10,11]. Nevertheless, recent studies demonstrated how these limitations could be overcome by properly engineering the shell structure and shape [12–15]. In particular, core/shell structures consisting of a spherical CdSe core surrounded by an elongated CdS shell, namely CdSe/CdS dots-in-rods (DRs), were able to provide bright and spectrally narrow photoluminescence [16], high absorption, outstanding quantum yield [15], suppression of the single-dot photoluminescence blinking[17], reduction of the luminescence reabsorption [18] and remarkable ensemble polarization properties [14,19], thus resulting very promising candidates in display manufacturing applications.

The PLQY of spherical QDs is usually high in solution state but is greatly reduced when QDs are transformed in closely packed thin films. Conversely, the PLQY of CdSe/CdS DRs is maintained when these nanostructures are transformed in thin films, due to an effective suppression of non-radiative energy transfer between closely packed DRs. This effect is owed to the rod geometry, that makes the spatial distribution of light emitting primitives relatively far away from each other, thus effectively suppressing the nonradiative inter-QDs Förster resonant energy transfer (FRET) [20,21]. Moreover, the CdSe/CdS DRs surfaces can be further engineered by growing additional inorganic shells coated by organic molecules. The presence of a further inorganic shell allows to improve the performances of luminance and efficiencies [22], while the involvement of specific organic ligand grafted to the nanocrystals surfaces provides a surface trap states passivation [23,24] and improves the solubility of the CdSe/CdS in polymeric matrices, allowing for the fabrication of hybrid nanocomposites films exploitable as down-conversion filters for display manufacturing. Moreover, the modulation of the rods' thickness, the use of specific organic ligands and the formation of close-packed thin films are valid strategies to modify the PL lifetime [25].

In such a scenario, this paper focuses on a preliminary study to produce core/shell architectures able to successfully convert blue light in red emission. In particular, CdSe/CdS DRs are prepared by using a conventional fast hot injection reaction method to grow CdS layers onto CdSe QDs cores [14, 26]. Then, CdSe/CdS@CdS/OA DRs are obtained by growing an additional CdS shell coated by oleate (OA) molecules on CdSe/CdS DRs. The formation of such a further shell is accomplished by means of a seeded-growth approach, by using TOP-S and cadmium oleate ($Cd(OA)_2$) as sulfur and cadmium precursors, respectively. This method is based on the slow injection of the precursors that enables to achieve a control over the thickness of the additional shell [16].

The absorption and emission properties of such shaped nanostructures and the effects produced by additional shells on the optical features of the final materials are investigated by means of UV-Vis absorption and PL spectroscopies. The morphological features of the produced architectures are investigated by means of transmission electron microscopy analyses (TEM).

In the light of the results, the here reported strategies are promising to synthesize core/multiple shell CdSe/CdS@CdS/OA DRs showing uniform size and tunable shell thickness, as well as absorption and PL emission properties suitable to the future fabrication of efficient down-conversion filters. Therefore, the nanorods obtained by growing an additional CdS shell coated by OA molecules are incorporated within a polymethyl methacrylate (PMMA) matrix to fabricate hybrid nanocomposite films exploitable for color down-conversion processes. These PL features of such hybrid films convincingly indicate that the produced materials show the potential to be applied in the next generation of displays and lighting devices.

EXPERIMENTAL

Chemicals

Trioctylphosphine oxide (TOPO 99%), Trioctylphosphine (TOP, 97%), Octadecylphosphonic acid (ODPA, 99%) and hexylphosphonic acid (HPA, 99%) are purchased from Plasmachem. Cadmium Oxide (CdO, 99.5%), Selenium (Se, 99,99%),1-octadecene (ODE 90%), oleic acid (OA 90%), and Sulfur (99%) are purchased from Sigma-Aldrich.

Synthesis of CdSe QDs (Core)

In a 25 mL three-neck round-bottom flask, TOPO (3.0 g, 7.5 mmol), ODPA (0.280 g, 0.9 mmol) and CdO (0.060 g, 0.47 mmol) are added and heated to ca. 150°C. The solution is exposed under vacuum for 1 hour and then under argon for 20 minutes.

Subsequently, the solution is heated to 320°C to dissolve the CdO until it turns optically clear and colorless.

In the meanwhile, a TOP-Se solution (0.058 g, 0.73 mmol of Se in 433 µl of TOP) is prepared under inert conditions. The solution is stirred at 60°C until selenium is completely dissolved.

At this point, the system is heated to 380°C and 1.8 mL of TOP quickly are injected in the flask. The temperature is allowed to recover 380°C and then the TOP-Se solution is quickly injected in the flask.

Then, the heating mantle is immediately removed, and 2 mL of toluene are added to the solution

After the synthesis, the nanocrystals are purified, precipitating them with methanol and washed in toluene by centrifugation for 12 min at 12000 rpm. Finally, the nanoparticles are dissolved in 3 mL of TOP and stirred overnight under inert conditions.

Synthesis of CdSe/CdS DRs

In a 25 mL three-neck round-bottom flask, CdO (0.090 g, 0.47 mmol) are mixed in a flask together with TOPO (3.0 g, 7.5 mmol), ODPA (0.280 g, 0.9 mmol) and HPA (0.080 g, 0.42 mmol). The flask is heated at 150°C and the resulting solution is exposed under vacuum for about 1 hour, then, the system is heated to 380°C under nitrogen. In the meanwhile, a solution of sulfur (S) precursor and nanocrystals (TOP-S+CdSe) is prepared by dissolving S (0.120 g, 3.7 mmol) and 800 µL of the CdSe solution in 2.2 mL of TOP. As well as the temperature recovered to the value required for the injection, the TOP-S+CdSe solution is quickly injected in the flask. The nanocrystals are allowed to grow for 8 minutes after the injection, after which the heating mantle is removed.

After the synthesis process, the obtained CdSe/CdS DRs nanostructures are precipitated with methanol by centrifugation for 12 min at 12000 rpm, dissolved in 3 mL of chloroform and stored at 4°C.

Synthesis of CdS/OA Hybrid Shell

The additional CdS shell coated by OA molecules is grown by using a solution containing TOP-S and $Cd(OA)_2$ as sulfur and cadmium precursors respectively, through the following procedure.

A solution 2 M of TOP-S is prepared by dissolving S (0.120 g, 3.75 mmol) in TOP (1.8 mL). $Cd(OA)_2$ is produced by mixing in a three-neck flask 0.64 g of CdO (5 mmol), in 3.8 mL of OA and 5 mL ODE. The mixture is degassed under vacuum at 30 °C for 20 minutes and heated to 280 °C under argon. As the CdO dissolved to form a colorless solution, the mixture is cooled to 30 °C. At this stage, the TOP-S solution is injected in the flask and the mixture is left under stirring for 30 minutes. Then, the resulting solution is splitted equally and transferred in two syringes.

At this stage, 1.5 mL of the solutions containing the CdSe/CdS DRs nanoparticles are precipitated with methanol and dissolved in 2 mL of hexane. The obtained solution and 3 mL of ODE are into a three-necked flask and degassed at 30 °C for 15 min under vacuum. The temperature is raised to 200 °C under argon atmosphere and the solution of TOP-S and $Cd(OA)_2$ is injected using a syringe pump with injection rate of 0.125 mL/min.

After the first injection, 1 mL of final solution is collected and purified. As soon as the addition of precursors is completed, 1 mL of oleic acid is added to prevent the aggregation of the particles.

The nanostructures obtained after the injections are precipitated with isopropanol and washed in chloroform by centrifugation at 12000 rpm for 3 minutes. Few drops of acetonitrile are added to the solution to help the precipitate of the particles. The procedure is repeated 3 times and the final products are dissolved in 5 mL of chloroform and stored in the dark.

The solutions obtained after the first and the second injections are named as CdSe/CdS@CdS/OA_1 and CdSe/CdS@CdS/OA _2 samples, respectively.

Fabrication of the Hybrid Nanocomposites Films

To encapsulate the produced heterostructures within a polymer matrix, 30 µL of CdSe/CdS@CdS/OA_1 sample are added to 500 µL of a 200 mg/mL solution of PMMA in chloroform. The final mixture is stirred at room temperature for 30 minutes and used for the deposition of films by spin coating technique on quartz slides (20 x 10 mm^2) for optical characterization. The spinning procedure is performed by using a PoloSpin 150i/200i spin coater. The films are produced by dropping 80 µL of the solution on the substrates and by spinning for 45s at 1000 rpm with a max recipe speed of 1000 rpm.

Characterization

The optical properties of the samples are investigated by UV-Vis absorption and PL spectroscopies measurements.

UV-Vis absorption spectra are recorded on a Jasco V750 spectrophotometer in the spectral range of 300-800 nm, the integration time of 0.6 s and slit widths of 1.5 nm.

PL measurements are performed by using a Fluoromax 4 Plus (Horiba) spectrofluorometer equipped with Origin program for data acquisition and analysis in the spectral range from 475 to 700 nm. The typical excitation wavelength of λ_{exc} = 425 nm is used with a spectral bandwidth of 1.5 nm for both the excitations and emission monochromators. The curves are automatically corrected for the spectral response of the detector.

The morphological properties of the samples are investigated by TEM analysis.

For the TEM characterization, the of CdSe/CdS and CdSe/CdS@CdS/OA_1 DRs samples are diluted several times with chloroform to obtain a monolayer of nanoparticles visible on the TEM grid.

The Transmission Electron analyses are performed with a JEOL JEM-1400 Plus microscope operating at 120 kV.

Data Analysis

All the PL and UV-Vis spectra are elaborated with Origin program. The averaged particle size (D) of the CdSe nanocrystals is estimated from the UV-Vis spectra according to the empirical equation (1) derived as shown by Yu et al [27]:

$$D = (9.8127 \cdot 10^{-7}) \cdot \lambda^3 - (1.7147 \cdot 10^{-3}) \cdot \lambda^2 + 1.0064 \cdot \lambda - 194.84 \quad (1)$$

where λ is the wavelength of the first exciton peak. The values of λ and D are both expressed in nm.

The PL spectra are deconvoluted by using Gaussian functions to derive position, amplitude (FWHM) and integrated intensity (I) of the peaks.

The PLQYs of the obtained DRs are determined by comparing the integrated emission of the nanorods samples in chloroform with that of Rhodamine B in ethanol as a reference according to the equation [28]:

$$\Phi_x = \frac{I_x \cdot A_{st} \cdot n_x^2}{I_{st} \cdot A_x \cdot n_{st}^2} \cdot \Phi_{st} \quad (2)$$

The subscripts “x” and “st” denote sample and standard, respectively. "Φ represents the PLQY, I is the integrated intensity of the emission spectra, n is refractive index of the solvent, and A is the absorbance at the excitation wavelength of 425 nm, used to acquire the PL spectra. Φ_{st} is the photoluminescent quantum yield of Rhodamine B that is 0.49. Before measurement, all the samples are adjusted to a concentration with an absorption value below to 0.1 at the excitation wavelength of 425 nm.

The TEM images are analyzed by using ImageJ software.

RESULTS AND DISCUSSION

The synthesis of CdSe/CdS@CdS/OA DRs and the fabrication of the hybrid nanocomposites films are accomplished according to the Scheme 1. Spherical CdSe QDs are synthesized via hot-injection method. CdSe/CdS core/shell DRs are produced via a synthetic approach of fast hot-injection reaction by using CdSe QDs as seeds for the nucleation and growth of the CdS shell. The final CdSe/CdS@CdS/OA DRs are obtained by a seeded-growth approach based on the slow injection of cadmium and sulfur precursors to form an additional CdS shells coated by OA molecules on CdSe/CdS DRs. Finally, the obtained heterostructures are incorporated within a transparent polymeric matrix for the fabrication of luminescent nanocomposites films suitable for color down-conversion processes.

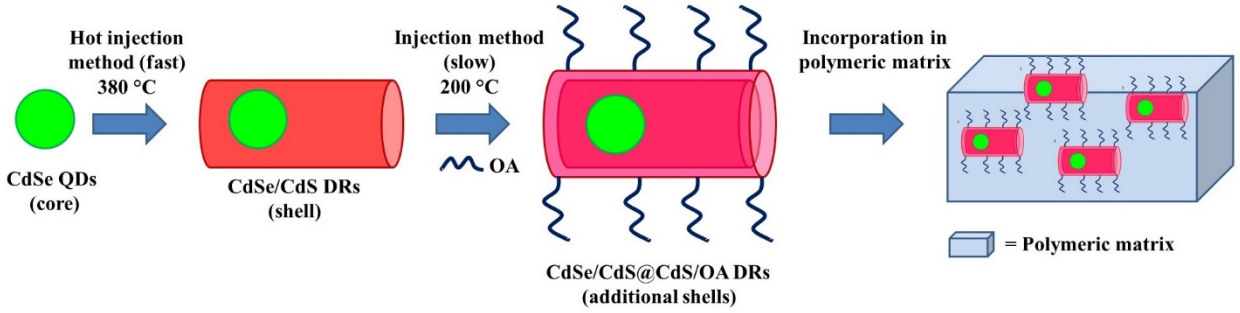

SCHEME 1. Scheme of the synthetic strategies to produce single (CdSe/CdS) and multiple shell (CdSe/CdS@CdS) DRs to be loaded within polymeric matrices for the fabrication of luminescent nanocomposites films. The surfaces of the multiple shell CdSe/CdS@CdS/OA DRs are coated by oleate (OA) molecules.

As indicated in the Scheme 1, the first step is the synthesis of spherical CdSe QDs. The absorption and PL emission spectra of CdSe nanocrystals are shown in Fig. 1 with the photograph of CdSe solution under UV lamp at 360 nm in the insert.

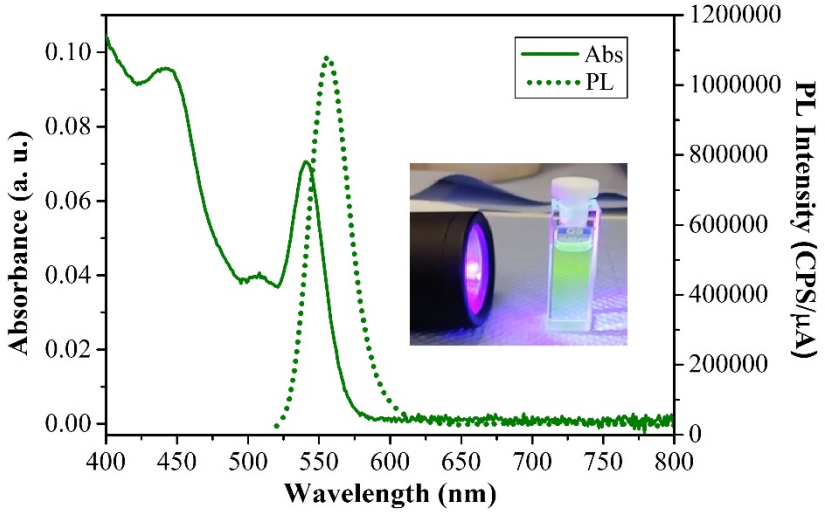

FIGURE 1. Absorption (straight line) and PL emission (dotted line) spectra of CdSe QDs. Inset: photograph of the CdSe solution under UV lamp at 360 nm.

As reported in Fig. 1 the absorption spectra of the CdSe QDs show a well distinct absorption maximum of the first electronic transition ($1S_{3/2}$ -$1S_e$) [29] at 532 nm. According to the equation (1), the absorption peak position allowed us to estimate an averaged dimension (D) of 2.9 nm for the produced nanocrystals. Regarding the emission properties, the PL peak is located at 555 nm, producing the emission of green light under an UV source at 360 nm,

as shown in the inset of Fig. 1. The sharp PL signal with a FWHM of 30 nm indicates the formation of nanocrystals with a narrow size distribution.

Given such considerations, the produced CdSe QDs are used as seeds for the nucleation and growth of the CdS rods.

In Fig. 2a is reported the TEM micrograph of CdSe/CdS DRs, that evidences the formation of elongated structures with a rod shape. To define the morphological features of the produced nanostructures, a statistical analysis estimated on 60 NPs.

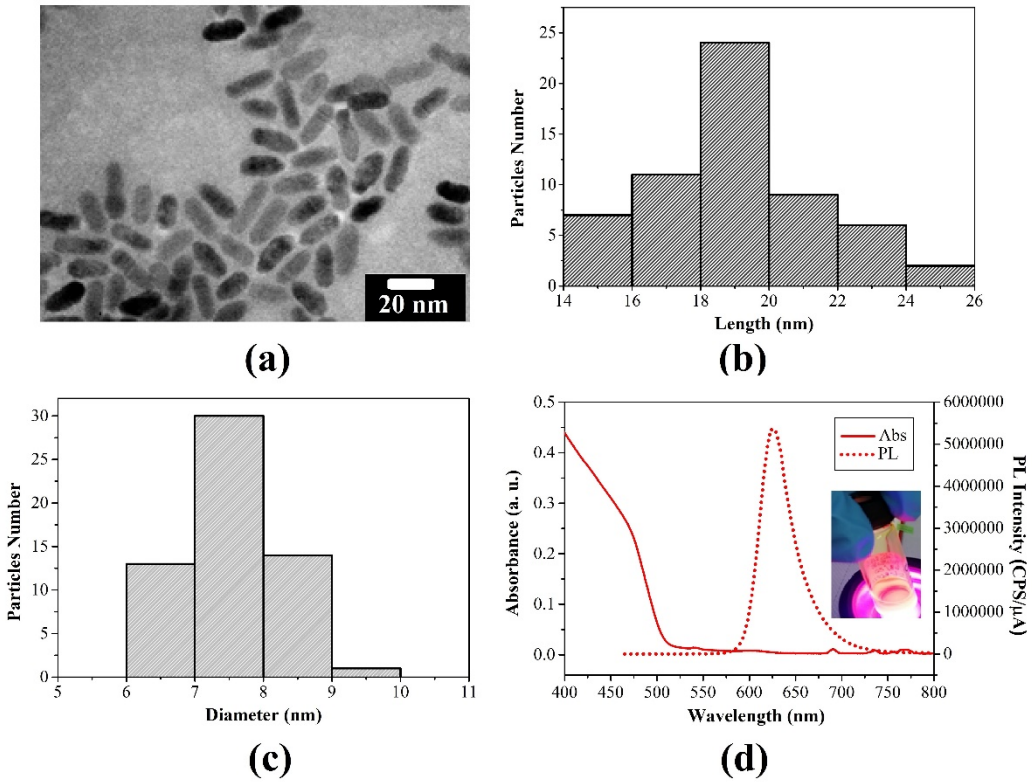

FIGURE 2. (a) TEM image of the CdSe/CdS DRs. Distribution of (b) length and (c) diameter of the rods. The data are estimated over 60 particles. (d) Absorption (straight line) and PL emission (dotted line) spectra of CdSe/CdS DRs. Inset: photograph of the CdSe/CdS DRs solution under UV lamp at 360 nm.

The TEM analysis indicates that the averaged length and diameter of the rods are 19.3 ± 2.6 nm (Fig. 2b) and 7.4 ± 0.8 nm (Fig. 2c), respectively. In particular, one can appreciate from the histogram reported in Fig. 2c that the distribution of diameters of the rods is fairly narrow. By taking into account the initial size of the core (D = 2.9 nm) and assuming 0.35 nm as the thickness of each individual CdS layer (half the wurtzite c unit cell parameter) [16,20], the number of CdS monolayers is estimated to be 12.

As shown in Fig. 2d, the absorption and PL spectra of the CdSe/CdS DRs exhibit well separated absorption and PL peaks, pointing out the growth of elongated structures. The formation of the CdS phase is indicated by the dominating absorption edge at around 480 nm, corroborating the presence of the energy band gap of nanosized CdS (2.56 eV) [19]. Given such a consideration, the shape of the absorption curve convincingly arises from the CdS rods. Comparing the PL spectrum of the CdSe/CdS DRs to that of the pristine CdSe QDs, the growth of the CdS shell produces a significant red shift in the peak position from 555 to 628 nm with an excitation source operating at 425 nm. The shift of about 70 nm is consistent with the formation of 12 CdS monolayers and is reasonably due to the lower confinement effect induced by the shell [16, 30]. Moreover, according to the equation (2), we calculated a PLQY around 50% for the produced CdSe/CdS DRs.

In this context, to improve the solubility of CdSe/CdS DRs in polymeric matrices for future applications in optical devices, additional hybrid CdS shells coated by OA molecules are grown by a seeded-growth approach based

on the slow injection of cadmium and sulfur precursors. The effects produced by the additional hybrid shells on the optical and morphological properties of the DRs are respectively investigated by optical absorption and PL spectroscopies and TEM analyses, as shown in Fig. 3

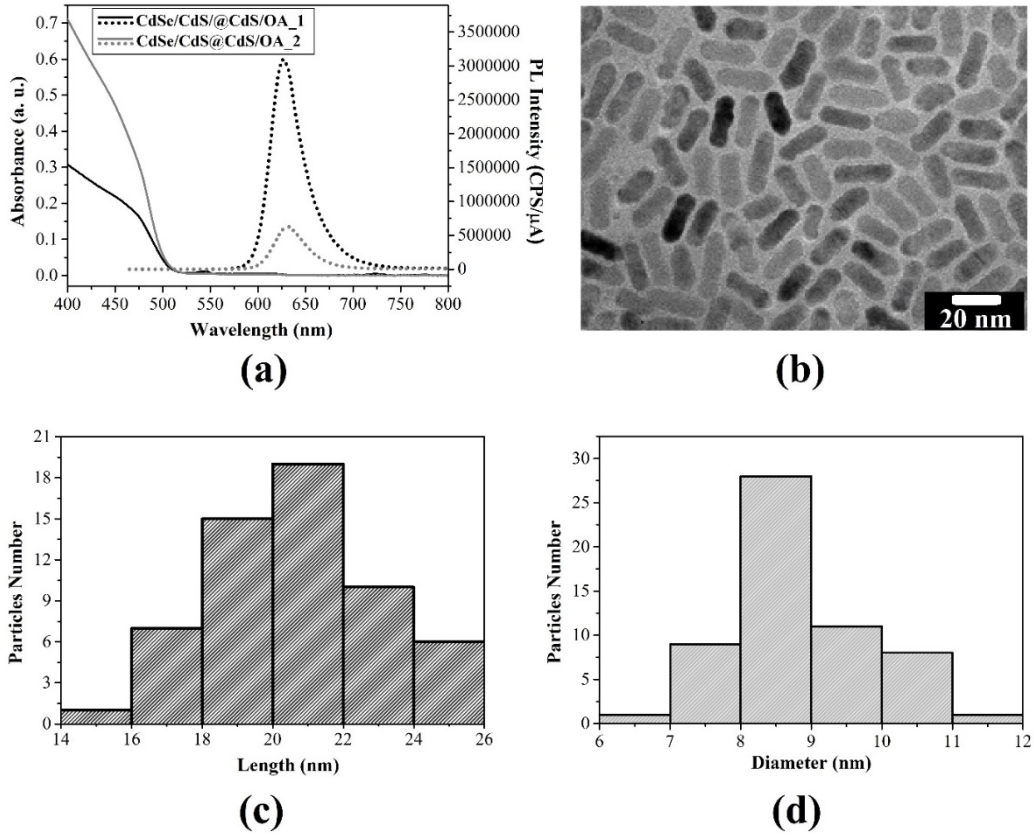

FIGURE 3. (a) Absorption (straight line) and PL emission (dotted line) spectra of aliquots taken during the addition of Cd/S precursors to a solution of CdSe/CdS DRs. (b) TEM image of the CdSe/CdS@CdS/OA_1 DRs. Distribution of (c) length and (d) diameter of the rods. The data are estimated over 60 particles.

The absorption and PL spectra of the nanostructures produced by the first (CdSe/CdS@CdS/OA_1 sample) and second (CdSe/CdS@CdS/OA_2 sample) injection are shown in Fig. 3a. Comparing these spectra with those of the pristine CdSe/CdS DRs (Fig. 2d), one can observe that the growing of additional CdS/OA hybrid shells produced no significant shifts neither in absorption nor in PL peaks. In particular, the PL signal remained at 628 nm with a sharp peak, suggesting the formation of rather monodisperse nanostructures. Regarding the PL emission efficiency, the PLQY decreases to 30% after the first injection of Cd/S precursor, reasonably ascribed to the increasing of the CdS shell thickness. Conversely, the PLQY of the CdSe/CdS@CdS/OA_2 sample drastically decreases to 6%, likely due to the long radiative lifetimes caused by delocalization of the electron into thicker shell [14,16].

Given such consideration, the morphological features of the materials produced after the first injection of the Cd/S precursors, namely CdSe/CdS@CdS/OA_1 sample, are investigated by TEM analysis.

At a first glance, in Fig. 3b one can observe that the growth of the hybrid shell by using small amounts of precursors maintained the elongated shape and the uniformity in length and width of the nanorods. This speculation is confirmed by a statistical analysis on 60 nanoparticles. As shown in the histogram reported in Fig. 4c the distribution of rods diameters remained quite narrow. In particular, the elaboration of the TEM images evidenced that the averaged length and diameter of the rods are 20.8 ± 2.7 nm and 8.9 ± 1.1 nm, respectively. Comparing these values to those of the pristine CdSe/CdS DRs and by assuming each layer of CdS had a thickness of 0.35 nm, the increasing of 1.6 nm in the shell volume indicates that further four CdS monolayers are grown over the pristine CdSe/CdS DRs. This finding indicates that the employed method allows to modulate the thickness of the nanorods.

Furthermore, the absorption and PL emission properties of the DRs produced by the addition further hybrid CdS/OA shell make these synthetic strategies valid for the engineering of nanocrystals surface. In addition, the PL lifetime of these heterostructures is expected to be around 30-40 ns and plausibly decreases after the incorporation in thin films, likely due to the prevention of non-radiative FRET [25].

In the light of the above reported considerations, the CdSe/CdS@CdS/OA_1 sample is loaded in a PMMA matrix to produce hybrid luminescent films exploitable for color down-conversion processes. In Fig. 4 are reported the normalized absorption and PL spectra of the CdSe/CdS@CdS/OA_1 film in comparison with those of the CdSe/CdS@CdS/OA_1 solution. In the inset, the photograph of the nanocomposite film under the UV lamp at 360 nm.

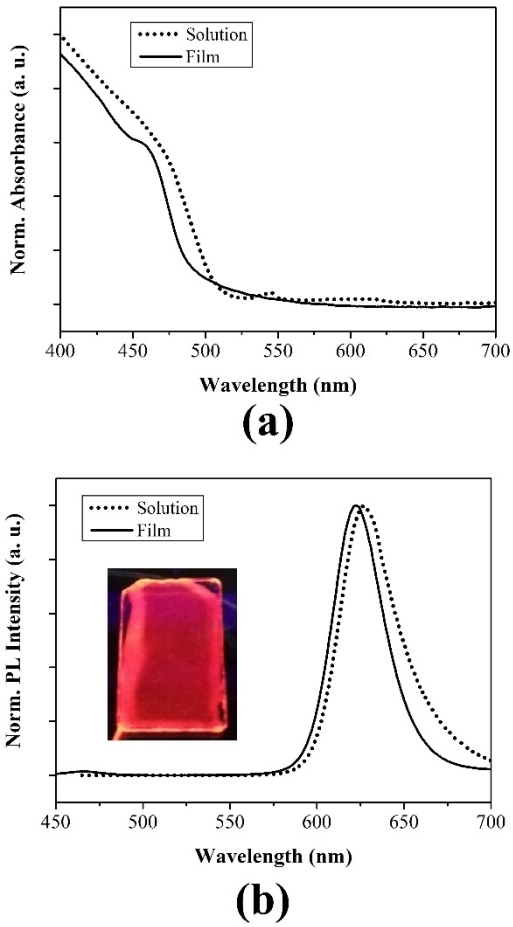

FIGURE 4. (a) Absorption and (b) PL emission spectra of CdSe/CdS@CdS/OA_1 DRs solution (dotted lines) and film (straight line). Inset: photograph of nanocomposite film under the UV lamp at 360 nm.

As shown in the inset of Fig. 4b, the CdSe/CdS@CdS/OA_1 sample is completely soluble within the polymeric mixture, enabling the formation of homogeneous nanocomposites films, emitting red light under UV lamp. The absorption and PL spectra of the film (straight line in Fig. 4a and 4b, respectively) confirmed that the luminescent properties are due to the CdSe/CdS@CdS/OA_1 heterostructures capsulated within the PMMA matrix. In particular, the absorption spectrum profile of the film reproduces that of the solution containing the CdSe/CdS@CdS/OA_1 sample (Fig. 4a), showing the absorption peak around 480 nm, typical of CdS structure. Regarding the PL properties, the position of PL peak in both of cases is maintained at around 628 nm, corresponding to the emission of red light (Fig. 4b). Analogously, the amplitude of the PL peak is 35 nm. In addition, we calculated a remarkable ratio between PL and absorbance intensity values, suggesting that the PLQY is maintained after the capsulation of

the CdSe/CdS@CdS/OA_1 heterostructures within the polymeric matrix. These findings convincingly indicate that the hybrid nanocomposite films are promising candidates for display manufacturing applications.

CONCLUSIONS

In conclusion, we reported a preliminary study based on a two-step method to produce heterostructures exploitable for the fabrication of lighting devices. The first step allows to grow elongated CdS shell on CdSe QDs cores by using a hot injection reaction, thus producing CdSe/CdS DRs with a high PLQY~ 50%, able to convert blue light in red wavelengths in down-conversion processes. However, display manufacturing applications require the incorporation of such inorganic systems in organic polymeric matrices to fabricate nanocomposite films.

Therefore, the second step consists of the slow high-temperature injection of TOP-S and $Cd(OA)_2$ to grow a hybrid inorganic/organic CdS/OA shell on the CdSe/CdS DRs surfaces. As assessed by TEM and absorption and PL spectroscopies analyses, the produced CdSe/CdS@CdS/OA DRs showed morphological and optical properties tunable as ~~a~~ function of the injected precursors amounts. In particular, the addition of small amounts of precursors produces heterostructures with optical features comparable to those of the pristine CdSe/CdS DRs.

The grafting of the OA molecules on the CdS surfaces improves the solubility of these nanostructures within the polymeric matrices, allowing for the fabrication of hybrid nanocomposites films required to be integrated in display manufacturing.

The optical features of the produced hybrid nanocomposites films indicate that these materials can convert blue light in red wavelengths, suggesting their usability for lighting applications.

These findings convincingly indicate that the strategies reported in this preliminary study produce materials that behave as promising candidates for the fabrication of down conversion filters for display manufacturing, as well as for advanced optoelectronic devices.

The achieved results foresee the possibility to extend the process to produce DRs able to emit green light after the excitation of a blue light pumping source.

ACKNOWLEDGMENTS

This paper is supported by European Union Horizon 2020 research and innovation programme (Photonics21, public private partnership) under Grant Agreement n 779373, project MILEDI (MIcro quantum dot Light Emitting diode and organic light emitting diodes DIrect patterning).

The authors thank Dr.ssa Rosa Maria Montereali, Head of Photonics Micro and Nanostructures Laboratory, ENEA Frascati, for her helpful advices and suggestions. The authors thank to Dr. Anatol Prudnikau and Prof. Vladimir Lesnyak (Technical University of Dresden) for their support on chemical synthesis, TEM analysis and helpful discussion.

REFERENCES

1. B. C. Krummacher, V. E. Choong, M. K. Mathai, S. A. Choulis, F. So, F. Jermann, T. Fiedler, and M. Zachau, Appl. Phys. Lett. **88**, 113506-113508 (2006).
2. S. Liu, X. Wen, W. Liu, W. Zhang, J. Yu, W. Xie, and L. Zhang, Curr. Appl. Phys. **14**, 1451-1454 (2014).
3. M. Yin, T. Pan, Z. Yu, X. Peng, X. Zhang, W. Xie, S. Liu, and L. Zhang, Org. Electron. **62**, 407- 411 (2018).
4. A. K. Srivastava, W. Zhang, J. Schneider, J. E. Halpert, and A. L. Rogach, Adv. Sci. **22**, 1901345 (1 of 20) (2019).
5. J. Li, Y. Liu, J. Hua, L. Tian, and J. Zhao, RSC Adv. **6**, 44859-44864 (2016).
6. S. J. Rosenthal, J. McBride, S. J. Pennycook, and L. C. Feldman, Surf. Sci. Rep. **62**, 111–157 (2007).
7. C. Murray, D. Norris, and M. Bawendi, J. Am. **115**, 8706–8715 (1993).
8. Z. A. Peng and X. Peng, J. Am. Chem. Soc. **123**, 183–184 (2001).
9. L. Qu, Z. A. Peng, and X. Peng, Nano Lett. **1**, 333–337 (2001).
10. R. G. Neuhauser, K. T. Shimizu, W. K. Woo, S. A. Empedocles, and M. G. Bawendi, Phys. Rev. Lett. **85**, 3301 - 3304 (2000).

11. G. Schlegel, J. Bohnenberger, I. Potapova, and A. Mews, Phys. Rev. Lett. **88**, 137401- 137404 (2002).
12. B. Mahler, P. Spinicelli, S. Buil, X. Quelin, J. P. Hermier, and B. Dubertret, Nat. Mater. **7**, 659-664 (2008).
13. J. Hu, L. S. Li, W. Yang, L. Manna, L. W. Wang, and A. P. Alivisatos, Science **292**, 2060-2063 (2001).
14. L. Carbone, C. Nobile, M. De Giorgi, F. Della Sala, G. Morello, P. Pompa, M. Hytch, E. Snoeck, A. Fiore, I. R. Franchini, M. Nadasan, A. F. Silvestre, L. Chiodo, S. Kudera, R. Cingolani, R. Krahne, and L. Manna, Nano Lett. **7**, 2942-2950 (2007).
15. F. Pisanello, L. Martiradonna, P. Spinicelli, A. Fiore, J. P. Hermier, L. Manna, R. Cingolani, E. Giacobino, M. De Vittorio, and A. Bramati, Superlattices Microstruct. **47**, 165-169 (2010).
16. I. Coropceanu, A. Rossinelli, J. R. Caram, F. S. Freyria, and M. G. Bawendi, ACS Nano **10**, 3295-3301 (2016).
17. T. Ihara, R. Sato, T. Teranishi, and Y. Kanemitsu, Phys. Rev. B - Condens. Matter Mater. Phys. **90**, 035309 (1 of 5) (2014).
18. M. Allione, A. Ballester, H. Li, A. Comin, J. L. Movilla, J. I. Climente, L. Manna, and I. Moreels, ACS Nano **7**, 2443-2452 (2013).
19. S. Deka, A. Falqui, G. Bertoni, C. Sangregorio, G. Poneti, G. Morello, M. De Giorgi, C. Giannini, R. Cingolani, L. Manna, and P. D. Cozzoli, J. Am. Chem. Soc. **131**, 817-812 (2009).
20. B. N. Pal, Y. Ghosh, S. Brovelli, R. Laocharoensuk, V. I. Klimov, J. A. Hollingsworth, and H. Htoon, Nano Lett. **12**, 331–336 (2012).
21. Z. Li, F. Chen, L. Wang, H. Shen, L. Guo, Y. Kuang, H. Wang, N. Li, and L. S. Li, Chem. Mater. **30**, 3668–3676 (2018).
22. Y. Zhang, F. Zhang, H. Wang, L. Wang, F. Wang, Q. Lin, H. Shen, and L. S. Li, Opt. Express **27**, 7935-7944 (2019).
23. N. Kirkwood, J. O. V. Monchen, R. W. Crisp, G. Grimaldi, H. A. C. Bergstein, I. Du Fossé, W. Van Der Stam, I. Infante, and A. J. Houtepen, J. Am. Chem. Soc. **140(46)**, 15712-15723. (2018).
24. F. Limosani, R. Carcione, and F. Antolini, J. Vac. Sci. Technol. B Nanotechnol. Microelectron. **38**, 012802 (1 of 9) (2020).
25. Zhang, Y., Zhang, F., Wang, H., Wang, L., Wang, F., Lin, Q., Shen, H., & Li, L. S., Optics express 27(6), 7935-7944 (2019).
26. L. Carbone and P. D. Cozzoli, Nano Today **5**, 449–493 (2010).
27. W. W. Yu, L. Qu, W. Guo, and X. Peng, Chem. Mater. **15**, 2854-2860 (2003).
28. J. Dimitrijevic, L. Krapf, C. Wolter, C. Schmidtke, J. P. Merkl, T. Jochum, A. Kornowski, A. Schüth, A. Gebert, G. Hüttmann, T. Vossmeyer, and H. Weller, Nanoscale **6**, 10413-10422 (2014).
29. A. I. Ekimov, I. A. Kudryavtsev, A. L. Efros, T. V. Yazeva, F. Hache, M. C. Schanne-Klein, A. V. Rodina, D. Ricard, and C. Flytzanis, J. Opt. Soc. Am. B **10**, 100-107 (1993).
30. M. G. Lupo, F. D. Sala, L. Carbone, M. Zavelani-Rossi, A. Fiore, L. Lüer, D. Polli, R. Cingolani, L. Manna, and G. Lanzani, Nano Lett. **8**, 4582–4587 (2008).